AIP Review of Scientific Instruments

High throughput optical readout of dense arrays of nanomechanical systems for sensing applications

N. F. Martínez, P. M. Kosaka, J. Tamayo, J. Ramírez, O. Ahumada et al.

Citation: Rev. Sci. Instrum. **81**, 125109 (2010); doi: 10.1063/1.3525090
View online: http://dx.doi.org/10.1063/1.3525090
View Table of Contents: http://rsi.aip.org/resource/1/RSINAK/v81/i12
Published by the American Institute of Physics.

Related Articles

A nano-cheese-cutter to directly measure interfacial adhesion of freestanding nano-fibers
J. Appl. Phys. 111, 024315 (2012)

Stabilization and growth of non-native nanocrystals at low and atmospheric pressures
J. Chem. Phys. 136, 044703 (2012)

Nanoparticle production in arc generated fireballs of granular silicon powder
AIP Advances 2, 012126 (2012)

Stability and topological transformations of liquid droplets on vapor-liquid-solid nanowires
J. Appl. Phys. 111, 024302 (2012)

Role of RuO3 for the formation of RuO2 nanorods
Appl. Phys. Lett. 100, 033108 (2012)

Additional information on Rev. Sci. Instrum.

Journal Homepage: http://rsi.aip.org

Journal Information: http://rsi.aip.org/about/about_the_journal

Top downloads: http://rsi.aip.org/features/most_downloaded

Information for Authors: http://rsi.aip.org/authors

ADVERTISEMENT

Explore AIP's new open-access journal

• Article-level metrics now available

• Join the conversation! Rate & comment on articles

Submit Now

Downloaded 30 Jan 2012 to 161.111.180.103. Redistribution subject to AIP license or copyright; see http://rsi.aip.org/about/rights_and_permissions

High throughput optical readout of dense arrays of nanomechanical systems for sensing applications

N. F. Martínez,[1,a] P. M. Kosaka,[2,a] J. Tamayo,[2] J. Ramírez,[1,3] O. Ahumada,[1] J. Mertens,[1] T. D. Hien,[4] C. V. Rijn,[4] and M. Calleja[2,b]
[1]*Mecwins S.L. Santiago Grisolía 2 (PTM), Tres Cantos, 28760 Madrid, Spain*
[2]*Instituto de Microelectrónica de Madrid, CSIC. Isaac Newton 8 (PTM), Tres Cantos 28760 Madrid, Spain*
[3]*Departamento de Ingeniería Química, ETSII/UPM, José Gutiérrez Abascal 2, 28006 Madrid, Spain*
[4]*Nanosens, Berkelkade 11, NL 7201 JE Zutphen, The Netherlands*

(Received 5 October 2010; accepted 15 November 2010; published online 28 December 2010)

We present an instrument based on the scanning of a laser beam and the measurement of the reflected beam deflection that enables the readout of arrays of nanomechanical systems without limitation in the geometry of the sample, with high sensitivity and a spatial resolution of few micrometers. The measurement of nanoscale deformations on surfaces of cm^2 is performed automatically, with minimal need of user intervention for optical alignment. To exploit the capability of the instrument for high throughput biological and chemical sensing, we have designed and fabricated a two-dimensional array of 128 cantilevers. As a proof of concept, we measure the nanometer-scale bending of the 128 cantilevers, previously coated with a thin gold layer, induced by the adsorption and self-assembly on the gold surface of several self-assembled monolayers. The instrument is able to provide the static and dynamic responses of cantilevers with subnanometer resolution and at a rate of up to ten cantilevers per second. The instrumentation and the fabricated chip enable applications for the analysis of complex biological systems and for artificial olfaction. © *2010 American Institute of Physics*.
[doi:10.1063/1.3525090]

I. INTRODUCTION

In the last ten years, nanomechanical systems have been increasingly used as mechanical transducers of chemical interactions as well as of biomolecular recognition events.[1–6] The most simple and widely used nanomechanical system is a microcantilever. The adsorption of a substance on a microcantilever significantly alters its vibration features and static deformation. The eigenfrequencies of the microcantilever are shifted due to the mass and mechanical stiffness of the adsorbate.[7–12] The static deformation originates as the outcome of intermolecular interactions between the adsorbed molecules themselves and their interaction with the surface of the microcantilever. Depending on the free surface energy variation and the dimensions and mechanical properties of the cantilever, molecular adsorption typically induces cantilever displacements from few to hundreds of nanometers. Therefore, techniques able to measure these displacements with subnanometer accuracy in bandwidths of 1 Hz are required. Main techniques for the readout of the nanomechanical response include the optical lever method,[13] interferometry-based methods,[14,15] integrated optical waveguides,[16,17] capacitive read-out,[18,19] and the use of piezoresistive cantilevers.[20–23] The optical lever is the most widespread method because of its simplicity, extreme sensitivity, and the capability for measuring in vacuum, air, gas mixtures, and liquids.[5] The sensing applications include detection of gases,[24] disease biomarkers,[25–27] pollutants,[28,29] explosives,[30,31] cells,[32] oligonucleotide sequences,[33–35] and pathogens.[32,36–38]

The growing interest in nanomechanical sensing is motivated by its ability for label-free detection, its high sensitivity, and the small sensor area that guarantees low reagent and sample consumption. On the other hand, disposable arrays of tens, or even hundreds of cantilevers can be mass produced at low cost by adopting well-established microfabrication techniques used in the semiconductor industry in the last decades.[39,40] Arrays of microcantilevers allow the simultaneous detection of tens of targets, which is demanding for the development of artificial noses, biochemical assays, early disease detection, and prognosis of diseases. Also, cross-sensitivities can be significantly minimized by using cantilever arrays by measuring the differential cantilever bending with respect to one or several cantilevers acting as references.[4,33] The implementation of arrays of nanomechanical sensors for complex biological and chemical analysis requires of suitable readout instrumentation with high sensitivity, high throughput, and flexibility for measuring with no constraints in the geometry and size of the cantilever arrays.

Parallel readout of microcantilever arrays has been achieved by integration of piezoresistive sensors and circuitry in the cantilevers themselves.[41,42] The main advantage of this method is that external alignment is unnecessary. The principal drawbacks are the electrical noise, Joule heating, and the need for the isolation of the electrical contacts in liquids. Also, the fabrication of dense arrays of piezoresistive cantilevers is technologically demanding despite advances in the arraying of electroactuated microcantilevers.[43] Alternatively, researchers have implemented the optical lever technique in a sequential way for the readout of microcantilever arrays.

[a]These authors equally contributed to this work.
[b]Author to whom correspondence should be addressed. Electronic mail: mcalleja@imm.cnm.csic.es.

 © 2010 American Institute of Physics

Downloaded 30 Jan 2012 to 161.111.180.103. Redistribution subject to AIP license or copyright; see http://rsi.aip.org/about/rights_and_permissions

Thus, the laser beams from an array of multiplexed laser emitters are focused on the free end of each microcantilever of the array, and the reflected laser beams are collected sequentially into a position sensitive photodetector[44] (PSD). This optical technique is able to measure several cantilevers per second with a resolution of 0.1 nm/Hz$^{1/2}$. However, the implementation is technologically demanding, mainly due to the alignment difficulties and the high density of components required, so only few (typically eight) cantilevers are integrated in the same array. Multiple laser emitters have also been used to detect the cantilever displacement at several locations along the cantilever surface and thus determine the curvature of the microcantilevers.[45] Other authors have preferred to fabricate cantilevers with an almost flat pad at the free end that provides a well defined reflected beam.[46] Hence, a collimated laser light beam with an expanded spot size illuminated the whole cantilever array. The laser light reflected off each cantilever's end pad was collected as an array of "spots" by a charge coupled device (CCD). This technique requires of a rigid paddle acting as a flat mirror on the free cantilever's end and the separation between cantilevers is limited to avoid the overlapping of reflected beams on the CCD. In addition, the bandwidth of the CCDs limits the measurement of the resonant frequency. Other researchers have applied optical interferometry.[47,48] However, this method requires that each cantilever contains a phase sensitive diffraction grating consisting of a reference and movable set of interdigitated fingers. Phase shifting and white light interferometry have proved to be a solution suitable for full-field characterization of the dynamic and static responses of cantilever arrays with no constraints in their geometry.[49–52] However, for sensing applications, the displacement resolution is somewhat limited (above a nanometer), and the acquisition time and image processing exceed tens of seconds for the static information, and tens of minutes for the dynamic data.[52] Laser-Doppler vibrometry possesses high potential for dynamic measurements of cantilever arrays; however, it does not provide information about the static deformation.[53]

In this work, we present a simple and robust technique for the optical readout of displacements of cantilever arrays with subnanometer accuracy, with no limitation in the geometry of the arrays and a spatial resolution of few micrometers. The optical alignment and search for the active mechanical sites are automatically done with minimal user intervention. The instrument is based on the scanning of a laser beam and the optical lever technique.[54,55] The technique provides a readout rate of tens of cantilevers per second that can be increased up to a hundred cantilevers per second. The displacement resolution of the method is of 0.01 nm/Hz$^{1/2}$.[55] It can be applied to dense arrays of cantilevers, and heterogeneous combinations of cantilever arrays. In addition, the measurement of the vertical displacements can be obtained at several positions along the cantilever, and thus, absolute cantilever profiles can be obtained. This feature allows the *ex situ* analysis and a comparison of the measurements after different sensitization and molecular recognition steps are performed outside the measurement setup. To exploit the potential of the readout technique, we have fabricated a chip consisting of a two-dimensional (2D) array of 128 cantilevers distributed in 16 separate reaction wells (Nanosens, the Netherlands). As a proof of concept, we show the nanomechanical response of these cantilevers upon the adsorption of self-assembled monolayers.

II. INSTRUMENT, MATERIALS AND METHODS

A. Sensor array

The starting material is a 4 in., (100)-oriented, double-side polished semiconductor-on-insulator (SOI) wafer with a thickness of 410 μm (from Icemos Technology, UK). The nominal thicknesses of the device and buried oxide (BOX) layers are 1000 and 400 nm, respectively. Standard microlithography process was carried out to define the cantilever patterns on a photoresist layer in the front-side of the wafer, followed by reactive ion etching (RIE) of the silicon device layer. The reactive etching gases were a mixture of SF_6, CHF_3, and O_2, and the silicon etching rate is of 1 μm per minute. By time control and regular checking, the etching process is stopped when the BOX SiO_2 layer is reached. After the etching step, the photoresist is stripped in oxygen plasma to reveal the silicon cantilever patterns. A 100-nm thick layer of a low-stress silicon nitride layer (Si_3N_4) was then deposited on both sides of the wafer by low-pressure chemical vapor deposition (LPCVD). The Si_3N_4 layer is used as a protective layer for a subsequent KOH etching of silicon. A second standard microlithography process was carried out to define the reaction wells on a photoresist layer in the back side of the wafer. Then, a RIE using a mixture of CHF_3 and O_2 gases is performed to etch the Si_3N_4, followed by stripping of the photoresist layer in an oxygen plasma oven. The wafer was then immersed in 25% of KOH solution at 75 °C to etch the silicon from the back side of the wafer. The etching is stopped when the BOX layer is reached. Subsequently, the wafer was immersed in RCA solution (H_2O_2:HCl:H_2O of 1:1:5) at 80 °C for 30 min to remove residual KOH. Then, the SiN layer was removed by using 85% of phosphoric acid solution at 180 °C, followed by etching of the SiO_2 BOX layer in a buffered HF containing solution to reveal the free-standing silicon cantilevers. A 20 nm thick gold layer was deposited by thermal evaporation at a rate of 0.1 nm/s. Previously, an intermediate 2 nm thick chromium layer was deposited to enhance the adhesion between the gold layer and the cantilever. Finally, the cantilever-contained chips are manually separated from the processing wafer. Optical and scanning electron microscopy images of the array are shown in Fig. 1(a).

B. Optical readout system

The readout technique presented here combines the optical beam deflection method and the automated 2D scanning of a single laser beam by voice-coil actuators.[54,55] Figure 1(b) shows a schematic drawing of the instrument. A 3 mW red laser diode (Edmund Optics Ltd.) is mounted on two perpendicular linear voice coil actuators (Physik Instrumente GmbH & Co.) for 2D scanning of the cantilever array. Voice coil actuators are based on the Lorentzian force between a radial field created by permanent magnets embedded on the inside

Downloaded 30 Jan 2012 to 161.111.180.103. Redistribution subject to AIP license or copyright; see http://rsi.aip.org/about/rights_and_permissions

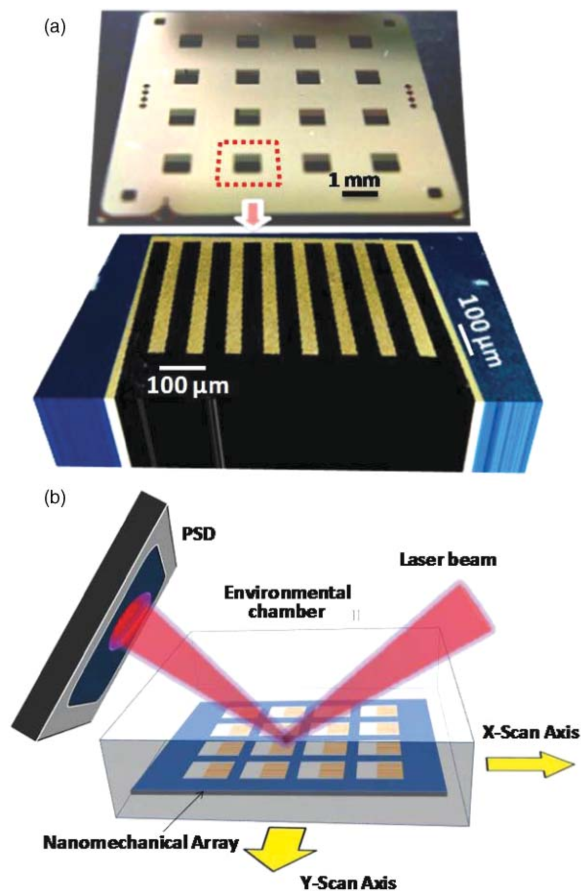

FIG. 1. (Color online) (a) Designed chip with 16 reaction wells of eight cantilevers each. The cantilevers were fabricated in single crystalline silicon. The nominal length, width, and thickness of the cantilevers were 400, 50, and 1 μm, respectively. A 20 nm thick gold layer was deposited by thermal evaporation on the top cantilever side. (b) Sketch of the system. The cantilever chip is mounted in a 2D voice-coil actuator for the displacement of the chip in the *X* and *Y* plane directions. The *X*-scanning direction is approximately along the cantilever longitudinal axis. Hence, the out-of-plane displacement of the nanomechanical system is along the *Z* axis. The incident laser beam is in the *X*–*Z* plane, and the PSD is oriented orthogonally to the reflected laser beam and with one axis in the *X*–*Z* plane. In this configuration, the photocurrents along this PSD axis are linearly proportional to the slope of the cantilever along the *X* direction. Since the photocurrents are normalized with respect to the total photocurrent, the slope values are insensitive to intensity fluctuations and variations in the optical properties of the surface.

diameter of a ferromagnetic cylinder and a current-carrying coaxial tubular coil that moves along the axial direction. The force is proportional to the applied current to the coil. Conversely, a voltage proportional to the velocity is induced in the coil, allowing accurate readout of the position. The advantages of using voice coil actuators include nonhysteretic displacement, a scanning range of several millimeters, speeds of up to 50 mm/s and an accuracy of 100 nm.

In our setup, one of the scanning axes is oriented approximately parallel to the cantilever longitudinal axis. The laser beam reflected off the chips is collected by a 2D linear position sensitive photodetector (PSD). The photocurrents generated on the PSD are processed by a four-channel current amplifier system using a position sensing algorithm which provides three analog outputs that are directly proportional to the total light collected on the PSD and to the two-dimensional coordinates of the reflected laser spot on the PSD, independently of any light intensity fluctuations.

The measurement process of the presented instrument consists of two steps. The aim of the first step is to determine the positions and orientations of all the cantilevers in the system. To this end, the laser beam sequentially scans all the cantilevers in the perpendicular direction to their longitudinal axes. The purpose of this scan is to determine the position of the edges of each microcantilever. This is achieved by on the fly analysis of the intensity signal of the reflected laser beam on the PSD as a function of the laser position. Edge detection is a nontrivial task, and there are several methods available in the field of artificial vision, such as computation of discrete gradients of intensity and application of a threshold. Once the position of the edges is available, the center of the cantilever is obtained as the middle point between the two edges. To obtain an accurate determination of the longitudinal axis of the cantilever, the midpoint is measured at different positions along the cantilever. Finally, the axis is obtained as the best fit to all the midpoints found per cantilever. Once the cantilever longitudinal axes have been detected, a new edge detection round is used to determine the position of the cantilever end and also the clamping point. This first stage takes a few minutes for our 2D cantilever arrays, but it has the following advantages: (i) it must be done only once at the beginning of the measurement, (ii) it can be extended to an arbitrary number of arrays with any number of cantilevers, and even to heterogeneous mixtures of chips with different number of cantilevers, (iii) it is very robust and allows to determine the positions and orientations of the cantilevers very accurately, automatically correcting for any possible optical misalignments, with no need of user intervention. The ultimate goal is the selection of the cantilevers to be monitored during the experiment.

During the second step, corresponding to the actual experiment, all the cantilevers, whose axes have been stored previously, are scanned sequentially in a step-like manner, by applying velocities of about 10 mm/s in the regions between cantilevers, and by stopping 1–10 ms at the free end of the cantilevers to determine its deflection with low noise.[55] This operation mode is used for experiments in real time, in which the cantilever response to environmental changes (temperature, relative humidity, molecular adsorption) is investigated. The readout rate can be of up to 100 cantilevers per second, and the performance of the sensors is not affected by the parallel read-out, as noise is limited by thermomechanical fluctuations.

Alternatively, the entire profile of the microcantilevers can be obtained by measuring the beam deflection at several locations along the cantilever and the nearby chip.[54] Since the beam-deflection technique is sensitive to the slope of the surface, the cantilever profile can be obtained by numerical integration of the PSD signal along the cantilever. A well known one-dimensional differential equation that relates the position $s(x)$ of the reflected laser beam on the PSD with the out-of-plane displacement of the cantilever $z(x)$ along the longitudinal position, x, is given by

$$s(x) \cong s_0 + 2d\frac{dz}{dx}(x) + x\cos\beta, \tag{1}$$

Downloaded 30 Jan 2012 to 161.111.180.103. Redistribution subject to AIP license or copyright; see http://rsi.aip.org/about/rights_and_permissions

where s_0 is an arbitrary offset position, d is the distance between the cantilever and the PSD, and β is the angle between the incident laser beam and the cantilever at its nondeflected position. The second term on the right hand side accounts for the effect of the laser beam displacement in the x direction that produces a translation of the reflected beam spot on the PSD. Integrating Eq. (1), the cantilever deflection as a function of x is obtained:

$$z(x) = \frac{1}{2d}\int_0^x [s(x') - s_0]dx' - \frac{1}{4}\frac{x^2}{d}\cos\beta. \tag{2}$$

To attain the absolute cantilever displacements, the values of s_0 and β must be determined. The instrument prior to the cantilever readout, performs a scanning of a flat region of the chip that is adopted as a reference, i.e., the changes of slope and height are calculated with respect to the mean height and slope of this region. Hence, the fitting of the region height with respect to a parabolic surface provides the values of s_0 and β.

C. Environmental chamber

The platform has an environmental chamber that allows the control of temperature (T) and relative humidity (RH). This is achieved by two closed-loop feedback mechanisms operating simultaneously on T and RH. The temperature control system is implemented with a standard PT-100 probe (sensor) located close to the cantilevers and two Peltier actuators (Supercool) placed in opposite sides of the measurement chamber. One of the Peltier cells is used for heating, whereas the other is used for cooling. An on–off algorithm implemented in LABVIEW (National Instruments) is used to vary the chamber and cantilever temperature from 288 to 313 K and to keep the temperature constant with an accuracy of 0.1 K.

The RH control system is implemented with a humidity probe from Hygrosens (sensor) and two mass-flow controllers (MFC) from Aalborg. The measurement chamber has an inlet for dry/wet gas (in our experiments is N_2). One of the MFCs provides a flow of dry N_2, and the other one provides a flow of wet N_2. Wet N_2 is obtained by passing the gas through a washing bottle from Schott-Duran. Both gas lines are mixed before reaching the measurement chamber. The algorithm implemented in LABVIEW regulates the flow rate of each MFC to reach the desired relative humidity in the chamber with an accuracy of 0.2%. In addition, it is capable of performing RH ramps from 0% to 100%.[35]

D. Self-assembled monolayer immobilization

All the used chemicals were analytical grade. 6-Mercapto-1-hexanol—97% [$HSCH_2(CH_2)_4CH_2OH$], 11-mercapto-1-undecanol—97% [$HSCH_2(CH_2)_9CH_2OH$], 9-Mercapto-1-nonanol—96% [$HSCH_2(CH_2)_7CH_2OH$], 1-dodecanethiol—$\geq$98% [$HSCH_2(CH_2)_{10}CH_3$], and 1-octadecanethiol—98% [$HSCH_2(CH_2)_{16}CH_3$] were purchased form Aldrich. We prepared 1 mM solution of each alkylthiol in distilled water. The 1 mM solutions of 11-mercapto-1-undecanol and 1-octadecanethiol were sonicated for 15 min. Prior to the formation of the self-assembled monolayers, the gold-coated chips were exposed to a freshly prepared H_2SO_4/H_2O_2 solution (piranha solution) for 5 min, rinsed three times with abundant distilled water and dried under a stream of dry N_2. The chip was placed in a controlled high humidity chamber and droplets of $\sim$2 μl of 1 mM of alkylthiol water solutions were placed in the reaction wells. After incubation, the array chip was rinsed three times with distilled water and dried under a stream of dry N_2.

III. CHARACTERIZATION OF MICROCANTILEVER ARRAYS

The mechanical responsivity of a microcantilever to molecular adsorption depends on its dimensions and it may be affected by residual stress, fabrication defects and the roughness of the coatings. In large arrays of cantilevers, as those shown here, spatial heterogeneities on the factors named above can occur, and therefore the mechanical responsivity of the cantilevers of the array is usually not uniform. Variations of the spring constant values over a factor of two have been found in microcantilevers fashioned from the same wafer.[56] The main factors in these deviations are the variations in the thickness of the device and of the coatings. For instance, the thickness of silicon nitride or polysilicon layers on silicon wafers used for subsequent cantilever fabrication can vary up to 20% across the wafer. The use of SOI wafers (as here) for the cantilever fabrication significantly improves the thickness uniformity, but, even in these cases, deviations of 5%–10% can be found. On the other hand, the gold deposition methods, such as thermal evaporation, sputtering or electron bombardment, inherently give rise to significant thickness gradients due to the distance variations between the metal source and the surface. More importantly, small variations in the deposition conditions in these thin films induce changes in the surface nanostructure that lead to large variations in the residual stress and the response to molecular adsorption.[57]

In order to account for the deviations of the mechanical properties of the cantilevers, we have measured with the presented instrument the resonance frequency and the variations of the cantilever profile to temperature variations. Figures 2(a) and 2(b) show the histograms of the values of the resonance frequency and cantilever deflection per temperature unit ($\Delta z/\Delta T$) for a 2D cantilever array. The mean value of the resonance frequency is 9.52 kHz, and the root mean square deviation is of 2.7%. The mean value of the deflection variation per temperature unit is of 75 nm/K, and the root mean square deviation is 11.2%. As shown below, the small deviation in the values of the resonance frequency indicates a good uniformity in the cantilever thickness. However, the significant deviation in $\Delta z/\Delta T$ suggests a nonuniform coating across the array. In Figs. 2(c) and 2(d), we show a color intensity map of the values of the resonance frequency and $\Delta z/\Delta T$ across the cantilever array chip. These maps are subsequently used to determine the responsivity of each cantilever to surface stress variations.

The angular resonance frequency[7] and cantilever deflection variation per temperature unit[58] are related to the cantilever dimensions and material properties by

Downloaded 30 Jan 2012 to 161.111.180.103. Redistribution subject to AIP license or copyright; see http://rsi.aip.org/about/rights_and_permissions

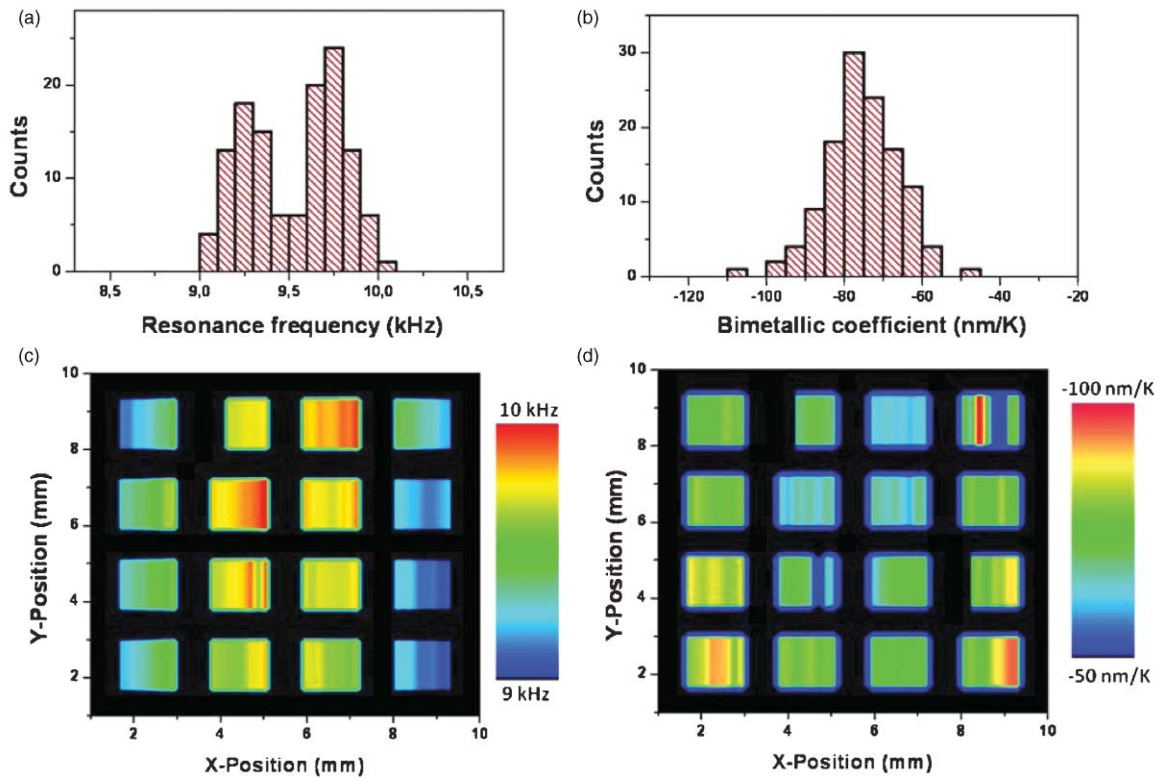

FIG. 2. (Color online) Histograms of the resonance frequency (a) and cantilever tip deflection per temperature unit (b) referred to as bimetallic coefficient of the gold-coated microcantilevers that comprise a 2D array. The frequency and bimetallic coefficient values of each cantilever in the chip are plotted as color intensity map in (c) and (d). The negative values of the bimetallic coefficient indicate that the cantilevers bend downwards toward the silicon side due to the higher thermal expansion coefficient of the gold.

$$\omega_0 \cong 1.015\sqrt{\frac{E_s}{\rho_s}}\frac{h_s}{L^2}\left[1+\frac{1}{2}\left(3\frac{E_f}{E_s}-\frac{\rho_f}{\rho_s}\right)\frac{h_f}{h_s}\right], \quad (3)$$

$$\frac{\Delta z}{\Delta T} \cong 3\frac{E_{f(1-\upsilon_s)}}{E_{s(1-\upsilon_f)}}(a_f - a_s)L^2\frac{h_f}{h_s^2}, \quad (4)$$

where E is Young's modulus, υ is Poisson's coefficient, ρ is mass density, L is cantilever length, α is thermal expansion coefficient, h is thickness, and the subscripts s and f refer to the cantilever substrate and coating film. Notice that the chromium layer has been neglected in the above equations for the sake of simplicity. Hence, the coating refers to the gold layer and the substrate to the silicon cantilever. By combining Eqs. (1) and (2), we calculate the mean values of the thickness of the cantilever and gold film, which are 1110 and 20.7 nm, respectively. These values are in a good agreement with the nominal values. The deviations in the thicknesses on each cantilever that constitute the two-dimensional array are plotted in Figs. 3(a) and 3(b). The root mean square deviations in the silicon and gold thicknesses are 2.5% and 9.9%, respectively.

Molecular adsorption induced surface stress (S) brings about a change of the cantilever curvature that is given by

$$\Delta K = 6\frac{1+2\frac{h_f}{h_s}\left(1-2\frac{E_f}{E_s}\frac{1-\nu_s}{1-\nu_f}\right)}{\frac{E_s}{1-\nu_s}h_s^2}S. \quad (5)$$

Equation (5) is the Stoney's equation[59] modified to account for the change of flexural rigidity and shift of the neutral bending axis due to the metallic layer.[7] By substituting the derived values of the thickness of the gold and silicon layers in Eq. (5), we calculate the cantilever tip deflection per surface stress change in each cantilever of the array [Fig. 3(c)]. The mean surface stress responsivity is 2.2 nm per mN/m, and the root mean square deviation is 4.7%. Since the gold layer is much thinner than the cantilever, the main source in the deviation of the mechanical responsivity is the deviation in the cantilever substrate thickness. In our case, this is of about 2.5% and arises from the deviation in the thickness of the silicon-on-insulator layer of the wafer supplied by the manufacturer, and used to fabricate the cantilevers. Although this deviation is small, the mechanical responsivity to surface stress has a square power dependence on the silicon thickness that results in a significant deviation. Therefore, a calibration of the mechanical properties of cantilevers is necessary prior to a chemical or biological assay to obtain quantitative values and, more importantly, to perform comparative analysis with cantilever arrays.

IV. APPLICATION: MOLECULAR ADSORPTION SENSING

In order to demonstrate the high multiplexing capability of the instrument for measuring molecular adsorption, we have tracked the deformation of the two-dimensional array of gold-coated microcantilevers previously calibrated in Sec. III. The chip contained 125 out of 128 entire cantilevers. Cantilever profiles have been calculated from the deflection of

Downloaded 30 Jan 2012 to 161.111.180.103. Redistribution subject to AIP license or copyright; see http://rsi.aip.org/about/rights_and_permissions

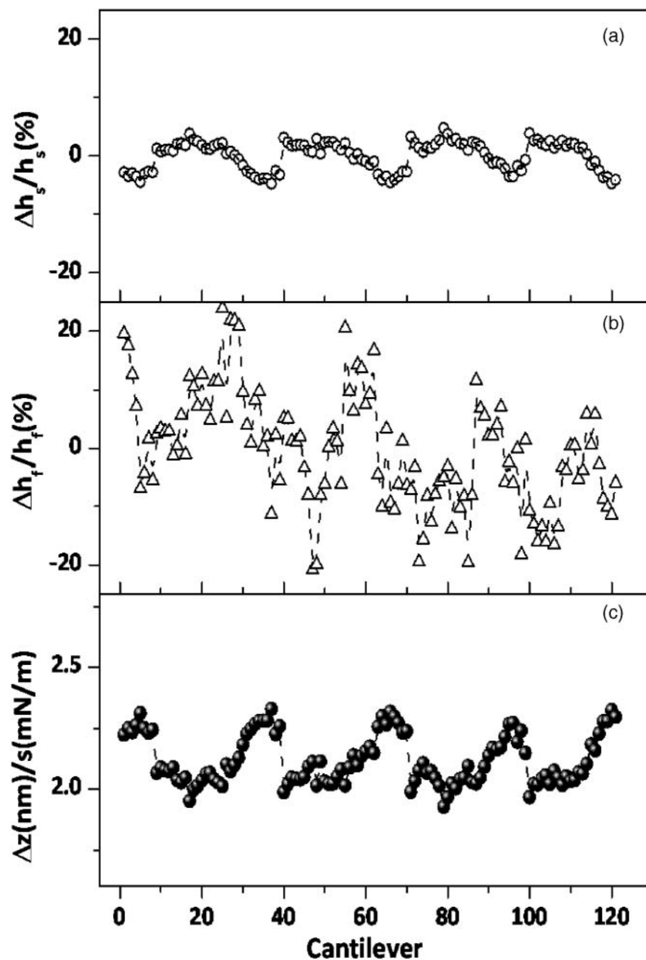

FIG. 3. Calculated values of the deviation in the thickness of the gold layer (a) and silicon substrate (b) of each cantilever comprising the array. The deviation is normalized by the mean value and expressed as percentage. The deviations are derived from the experimental values of the resonance frequency and deflection vs temperature shown in Fig. 2. (c) Calculated displacement of the cantilever tip induced by surface stress in each cantilever of the array (responsivity to surface stress). The response is derived from the calculated values of the thickness of the gold and silicon layers.

multiple points along cantilever length as described in Eqs. (1) and (2). Experimentally, a large scan of 1.2 mm is performed in the direction of the longitudinal axis of the cantilever. This scan covers 0.6 mm from the clamping position to the chip side and 0.6 mm away from clamping position to the cantilever free end. The signal acquired on the PSD for the 1.2 mm scan shows two clearly distinct regions, a flat region corresponding to the laser being reflected on the chip surface, and a second region showing a linear dependence $s(x) = \kappa x$, corresponding with the laser being reflected on the cantilever surface. A three dimensional image of the PSD signal across the chip is shown in Fig. 4(a). The linear dependence on the longitudinal position, x, indicates that the actual cantilever profile is parabolic $z(x) = \frac{1}{2}\kappa x^2$. To determine the curvature parameter of the cantilever profile, a linear regression is performed with the experimental data obtained from the PSD. The range of x-points included in the linear regression is $[0.1L - 0.9L]$, L being the total length of the cantilever. The linear regression is usually performed with at least 40 data points. From the obtained curvature values, we calculate the surface stress by using the values of the responsivity to surface stress previously obtained as shown in Sec. III.

As a proof of concept for molecular adsorption detection, we incubated the chip for 1 h with 1 mM 6-mercapto-1-hexanol (MCH) (purchased from Sigma-Aldrich) diluted in water. The chip was then vigorously rinsed with water and dried with dry nitrogen. MCH forms a self-assembled monolayer on the gold-coated side of the cantilevers due to the strong bond between the thiol terminal group and the gold and the attractive interactions between the alkyl chains. The measurements were performed *ex situ* in air at 24 °C and a relative humidity of 30%. We did not find a significant dependence of the cantilever response with the humidity. Figure 4(b) shows the cantilever tip displacements before and after MCH incubation. All the cantilevers bend toward the silicon side, which indicates the build-up of compressive surface stress in the gold layer. This is related to changes in the electronic charge density at the underlying metal's surface.[60–62] From the change of curvature, we calculated the surface stress. A histogram of the surface stress is shown in Fig 4(c). The mean surface stress variation was 125 mN/m, and the root mean square deviation was 25%. The deviation is relatively high, and it cannot be explained by the deviations in the mechanical properties of the cantilevers that are of 4.7% and, also, they have been taken into account for calculating the surface stress. The fluctuation of the surface stress is closer to the fluctuations found for the gold thickness and shown in Fig. 3(b). We previously found that small variations in the thickness of thin gold films can produce large deviations in the cantilever response to adsorption-induced surface stress. Gold films with a thickness of about 20 nm are discontinuous and consist of grains with a size of about 30–70 nm. The film nanostructure, grain size and shape, can change with a subtle variation of the thickness. For instance, the grains can be separated by well-defined grain boundaries or they can initiate coalescence, a process that leads to a reduction of the surface energy and is favored by the liquidlike behavior of the surface atoms for small grains.[63,64] These morphological changes have a high impact in the subsequent surface stress upon molecular adsorption.[57]

In a second experiment, we compare the surface stress induced by self-assembled monolayers of alkylthiols as a function of the head group and alkane chain length. In particular, we incubate 15 of the 16 reaction wells of the chip with mercaptohexanol, SH–$(CH_2)_6$–OH, mercaptononanol, SH–$(CH_2)_9$–OH, mercaptoundecanol, SH–$(CH_2)_{11}$–OH, dodecanethiol, SH–$(CH_2)_{11}$–CH_3, and octadecanethiol, SH–$(CH_2)_{17}$–CH_3. The first three alkylthiols are terminated in hydroxyl and the last two in methyl. Since the methyl group is nonpolar, and the alcohol is polar, hydroxyl terminated SAMs give rise to hydrophilic surfaces, whereas the methyl-terminated SAMs give rise to hydrophobic surfaces.[65] To obtain enough statistic information, each alkylthiol was incubated in three reaction wells of the chip overnight that comprises 54 cantilevers. The concentration was 1 mM.

In order to differentially functionalize cantilevers, a microfluid chamber was integrated at each reaction well [Fig. 5(a)]. The microfluidic chamber consisted of 16 wells as

Downloaded 30 Jan 2012 to 161.111.180.103. Redistribution subject to AIP license or copyright; see http://rsi.aip.org/about/rights_and_permissions

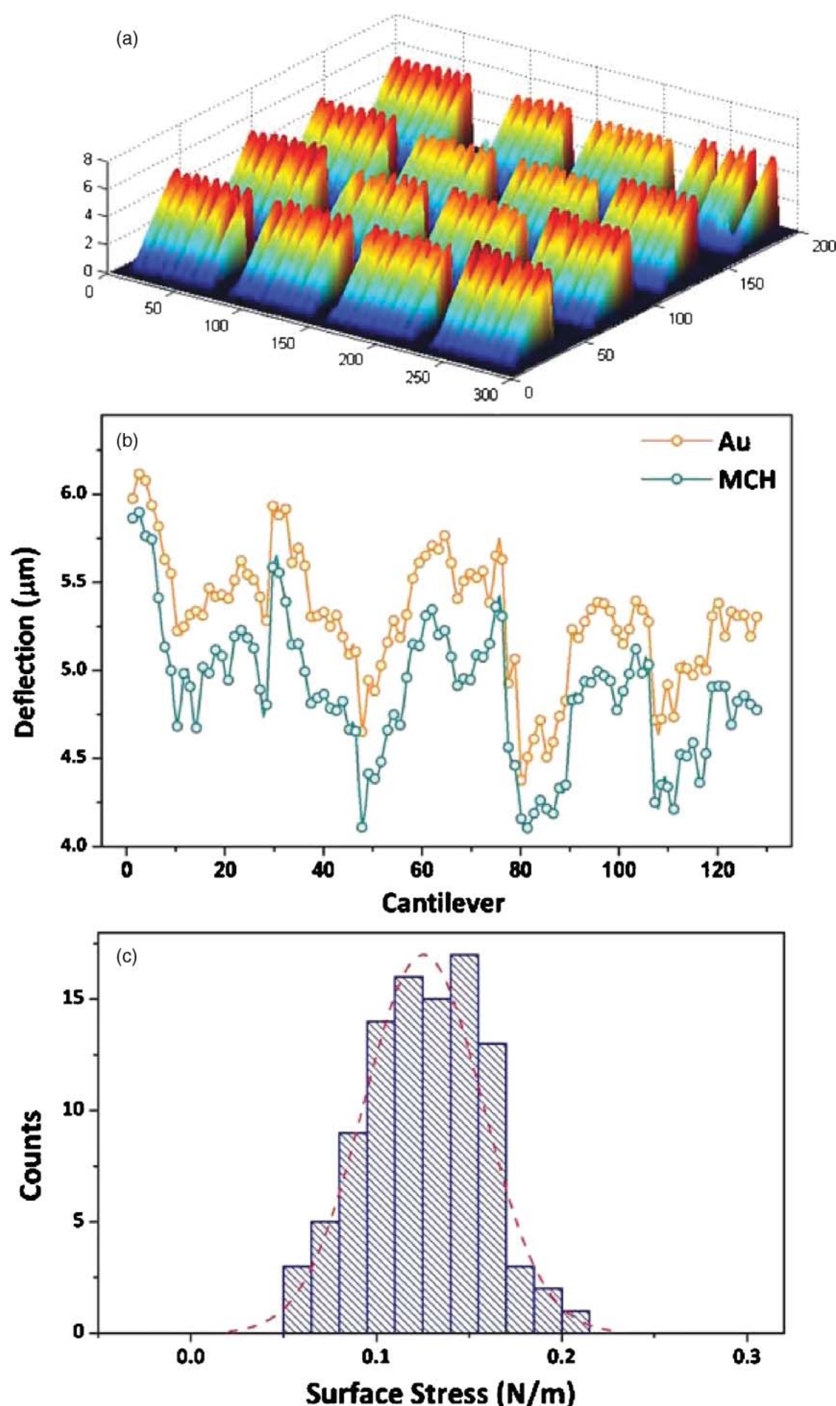

FIG. 4. (Color online) (a) 3D representation of the PSD signal corresponding to the cantilever slope along the longitudinal direction as a function of the *XY* position on the chip. (b) Cantilever displacement before and after incubation with MCH. After the formation of the self-assembled monolayer on the gold side, the cantilever bends toward the silicon side. (c) Histogram of the compressive surface stress induced by the MCH adsorption. The surface stress was calculated from the measured change of the cantilever curvature and using a modified Stoney's equation as explained in the main text.

those of the 2D cantilever array obtained by etching 725 μm thick bulk silicon and bonding it with a thin layer of polydimethylsiloxane elastomer (PDMS) with the same motifs. The cantilever and microfluidic chamber were then pressed against a bottom layer of silicon covered with PDMS. Liquid can be injected I/O port by micropipette. The full thickness of the well is of about 1.5 mm; therefore, each well carries a volume of 2.3 μl of sample solution. A photograph of the assembled chip with solution from different samples is shown in Fig. 5(b). No mixing or leakage has been observed between wells by performing fluorescence microscopy experiments.

Figure 5(c) shows the mean values of the surface stress as a function of the number of carbons of the alkane chain. In all cases, the surface stress is compressive, i.e., the gold film expands, and the cantilever bends toward the silicon side. Despite the relatively significant fluctuations of the surface stress, the large number of cantilevers used in the experiments allow to establish some relevant trends. As previously found

Downloaded 30 Jan 2012 to 161.111.180.103. Redistribution subject to AIP license or copyright; see http://rsi.aip.org/about/rights_and_permissions

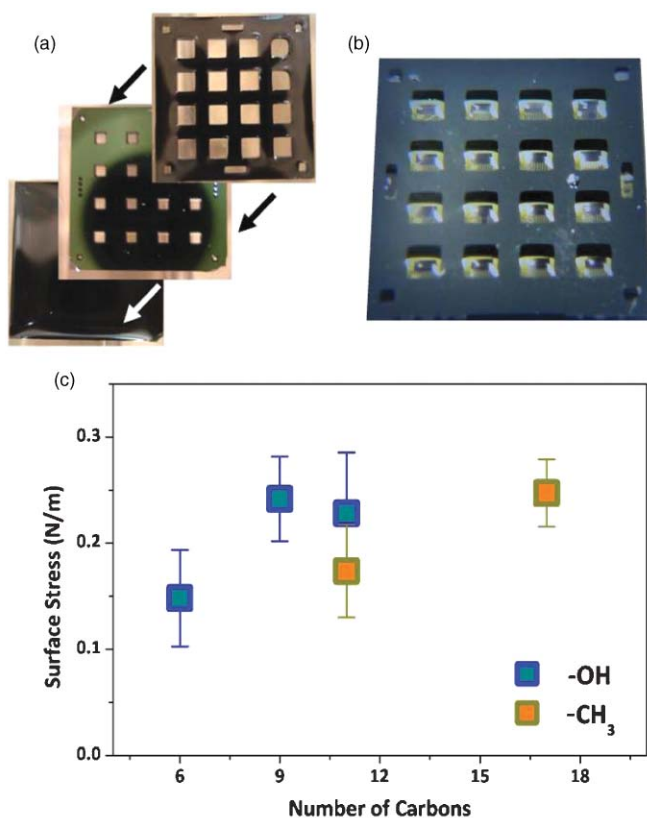

FIG. 5. (Color online) (a) Assembly of different parts of the cantilever and microfluidics chip. The microfluidic chamber consists of 16 wells, as those of the 2D cantilever, made of bulk silicon, and a thin layer of PDMS. The cantilever and microfluidic chamber are pressed against a bottom layer of silicon covered with PDMS. Liquid can be injected I/O port by micropipette. (b) A photograph of the assembled chip with solution from different samples. No mixing or leakage has been observed between wells. (c) Mean and deviation values of the compressive surface stress induced by the self-assembly of hydroxyl-terminated alkylthiols, SH–$(CH_2)_n$–OH, and methyl-terminated alkylthiols, SH–$(CH_2)_n$–CH_3, as a function of the alkane chain length n.

with alkanethiols on grainy gold films, the surface stress increases with the alkane chain length.[66] Whereas this increase was found in methyl-terminated alkylthiols from 4 to 14 carbon units, our preliminary data suggest that this increase also occurs with hydroxyl-ended alkythiols, although it saturates for chains longer than 9 carbon units. On the other hand, mercaptononanol and dodecanethiol that only differ in the headgroup show a significant difference in surface stress. The hydroxyl-terminated alkanethiols give more compressive surface stress than the corresponding methyl-terminated alkylthiol with the same length. Our data seems to have a relation with previous reports in which the authors observed that interaction between hydroxyl groups via hydrogen bonding leads to a higher stabilization of the self-assembled monolayer.[67,68]

V. CONCLUSION

We have presented an instrument for the surface inspection and read-out of hundreds of microcantilevers. The instrument allows fast acquisition and the capability to record the full 3D profile, as well as the resonance frequency of cantilever arrays of any size, shape, and number of elements. The chips are enclosed in an environmental chamber that enables control of temperature and humidity for quantitative *ex-situ* sensing experiments. The alignment of the laser beam and recognition of the microcantilever position are done automatically. The instrument has the advantage that any modification to the microcantilevers, like bioreactions, deposition of metal layers or molecular recognition experiments, can be performed *ex situ* while keeping the information of the surface stress induced by the modification. To exploit the high-thoughput capability of the instrument, we have designed and fabricated two-dimensional cantilever arrays comprising 128 cantilevers distributed in 4 × 4 reaction wells. The reaction wells allow individual functionalization of groups of eight cantilevers by integrating a microfluidic chamber, and hence to perform comparative biochemical assays. Here, as a proof of concept, we have tracked the curvature change of 128 microcantilevers upon adsorption of self-assembled monolayers. The instrument and the cantilever chips place at hand the fast and accurate parallel detection of tens of different analytes, which is demanding, for instance, for disease diagnosis and prognosis. In these applications, a profile of many biomarkers is more reliable and accurate than measuring only one or few disease markers.

ACKNOWLEDGMENTS

The authors acknowledge financial support from the Spanish Science Ministry through Project Nos. TEC2009–14517-C02, TRA2009–0117, and CSD2007–00010.

[1]M. Baller, H. Lang, J. Fritz, C. Gerber, J. Gimzewski, U. Drechsler, H. Rothuizen, M. Despont, P. Vettiger, and F. Battiston, Ultramicroscopy **82**, 1 (2000).
[2]J. Fritz, M. Baller, H. Lang, H. Rothuizen, P. Vettiger, and E. Meyer, Science **288**, 316 (2000).
[3]K. Ekinci and M. Roukes, Rev. Sci. Instrum. **76**, 061101 (2005).
[4]H. Lang, M. Hegner, and C. Gerber, Mater. Today **8**, 30 (2005).
[5]P. Waggoner and H. Craighead, Lab on a Chip **7**, 1238 (2007).
[6]M. Li, H. Tang, and M. Roukes, Nat. Nanotechnol. **2**, 114 (2007).
[7]J. Tamayo, D. Ramos, J. Mertens, and M. Calleja, Appl. Phys. Lett. **89**, 224104 (2006).
[8]D. Ramos, J. Tamayo, J. Mertens, M. Calleja, and A. Zaballos, J. Appl. Phys. **100**, 106105 (2006).
[9]D. Ramos, J. Tamayo, J. Mertens, M. Calleja, L. Villanueva, and A. Zaballos, Nanotechnology **19**, 035503 (2008).
[10]M. Spletzer, A. Raman, and R. Reifenberger, Appl. Phys. Lett. **91**, 184103 (2007).
[11]R. Grüter, Z. Khan, R. Paxman, J. Ndieyira, B. Dueck, B. Bircher, J. Yang, U. Drechsler, M. Despont, and R. McKendry, Appl Phys Lett. **96**, 023113 (2010).
[12]E. Gil-Santos, D. Ramos, J. Martínez, M. Fernández-Regúlez, R. García, Á. San Paulo, M. Calleja, and J. Tamayo, Nat. Nanotechnol. **5**, 641 (2010).
[13]G. Meyer and N. Amer, Appl. Phys. Lett. **53**, 1045 (1988).
[14]D. Rugar, H. Mamin, and P. Guethner, Appl. Phys. Lett. **55**, 2588 (1989).
[15]N. Azak, M. Shagam, D. Karabacak, K. Ekinci, D. Kim, and D. Jang, Appl. Phys. Lett. **91**, 093112 (2007).
[16]M. Nordström, D. Zauner, M. Calleja, J. Hübner, and A. Boisen, Appl. Phys. Lett. **91**, 103512 (2007).
[17]J. Noh, R. Anderson, S. Kim, J. Cardenas, and G. Nordin, Opt. Express **16**, 12114 (2008).
[18]Z. Davis, G. Abadal, B. Helbo, O. Hansen, F. Campabadal, F. Pérez-Murano, J. Esteve, E. Figueras, J. Verd, and N. Barniol, Sens. Actuators A **105**, 311 (2003).
[19]Y. Li, M. Ho, S. Hung, M. Chen, and M. Lu, J. Micromech. Microengrg. **16**, 2659 (2006).
[20]A. Boisen, J. Thaysen, H. Jensenius, and O. Hansen, Ultramicroscopy **82**, 11 (2000).

Downloaded 30 Jan 2012 to 161.111.180.103. Redistribution subject to AIP license or copyright; see http://rsi.aip.org/about/rights_and_permissions

[21]A. Johansson, M. Calleja, P. Rasmussen, and A. Boisen, Sens. Actuators A **123**, 111 (2005).
[22]B. Chui, T. Stowe, T. Kenny, H. Mamin, B. Terris, and D. Rugar, Appl. Phys. Lett. **69**, 2767 (1996).
[23]J. Arlett, J. Maloney, B. Gudlewski, M. Muluneh, and M. Roukes, Nano Lett. **6**, 1000 (2006).
[24]D. Raorane and A. Majumdar, Nano Lett. **8**, 2229 (2008).
[25]G. Wu, R. Datar, K. Hansen, T. Thundat, R. Cote, and A. Majumdar, Nat. Biotechnol. **19**, 856 (2001).
[26]Y. Arntz, J. Seelig, H. Lang, J. Zhang, P. Hunziker, J. Ramseyer, E. Meyer, M. Hegner, and C. Gerber, Nanotechnology **14**, 86 (2003).
[27]F. Huber, M. Hegner, C. Gerber, H. Güntherodt, and H. Lang, Biosens. Bioelectron. **21**, 1599 (2006).
[28]M. Alvarez, A. Calle, J. Tamayo, L. Lechuga, A. Abad, and A. Montoya, Biosens. Bioelectron. **18**, 649 (2003).
[29]C. Suri, J. Kaur, S. Gandhi, and G. Shekhawat, Nanotechnology **19**, 235502 (2008).
[30]L. Pinnaduwage, V. Boiadjiev, J. Hawk, and T. Thundat, Appl Phys Lett. **83**, 1471 (2003).
[31]L. Senesac and T. Thundat, Mater Today **11**, 28 (2008).
[32]T. Burg, M. Godin, S. Knudsen, W. Shen, G. Carlson, J. Foster, K. Babcock, and S. Manalis, Nature (London) **446**, 1066 (2007).
[33]R. McKendry, J. Zhang, Y. Arntz, T. Strunz, M. Hegner, H. Lang, M. Baller, U. Certa, E. Meyer, and H. Güntherodt, Proc. Natl. Acad. Sci. U.S.A. **99**, 9783 (2002).
[34]J. Zhang, H. Lang, F. Huber, A. Bietsch, W. Grange, U. Certa, R. McKendry, H. Güntherodt, M. Hegner, and C. Gerber, Nat. Nanotechnol. **1**, 214 (2006).
[35]J. Mertens, C. Rogero, M. Calleja, D. Ramos, J. Martín-Gago, C. Briones, and J. Tamayo, Nat. Nanotechnol. **3**, 301 (2008).
[36]B. Ilic, D. Czaplewski, M. Zalalutdinov, H. Craighead, P. Neuzil, C. Campagnolo, and C. Batt, J. Vac. Sci. Technol. B **19**, 2825 (2001).
[37]B. Ilic, Y. Yang, and H. Craighead, Appl. Phys. Lett. **85**, 2604 (2004).
[38]A. Gupta, D. Akin, and R. Bashir, Appl. Phys. Lett. **84**, 1976 (2004).
[39]P. Vettiger, M. Despont, U. Drechsler, U. Dürig, W. Häberle, M. Lutwyche, H. Rothuizen, R. Stutz, R. Widmer, and G. Binnig, IBM J. Res. Dev. **44**, 323 (2000).
[40]K. Salaita, S. Lee, X. Wang, L. Huang, T. Dellinger, C. Liu, and C. Mirkin, Small **1**, 940 (2005).
[41]L. Pinnaduwage, A. Gehl, S. Allman, A. Johansson, and A. Boisen, Rev. Sci. Instrum. **78**, 055101 (2007).
[42]G. Yoshikawa, H. Lang, T. Akiyama, L. Aeschimann, U. Staufer, P. Vettiger, M. Aono, T. Sakurai, and C. Gerber, Nanotechnology **20**, 015501 (2009).
[43]M. Lutwyche, M. Despont, U. Drechsler, U. Dürig, W. Häberle, H. Rothuizen, R. Stutz, R. Widmer, G. Binnig, and P. Vettiger, Appl. Phys. Lett. **77**, 3299 (2000).
[44]H. Lang, R. Berger, C. Andreoli, J. Brugger, M. Despont, P. Vettiger, C. Gerber, J. Gimzewski, J. Ramseyer, and E. Meyer, Appl. Phys. Lett. **72**, 383 (1998).
[45]S. Jeon and T. Thundat, Appl. Phys. Lett. **85**, 1083 (2004).
[46]M. Yue, J. Stachowiak, H. Lin, R. Datar, R. Cote, and A. Majumdar, Nano Lett. **8**, 520 (2008).
[47]S. Manalis, S. Minne, A. Atalar, and C. Quate, Appl. Phys. Lett. **69**, 3944 (1996).
[48]T. Sulchek, R. Grow, G. Yaralioglu, S. Minne, C. Quate, S. Manalis, A. Kiraz, A. Aydine, and A. Atalar, Appl. Phys. Lett. **78**, 1787 (2001).
[49]J. Wehrmeister, A. Fuß, F. Saurenbach, R. Berger, and M. Helm, Rev. Sci. Instrum. **78**, 104105 (2007).
[50]S. Kelling, F. Paoloni, J. Huang, V. Ostanin, and S. Elliott, Rev. Sci. Instrum. **80**, 093101 (2009).
[51]J. Reed, P. Wilkinson, J. Schmit, W. Klug, and J. Gimzewski, Nanotechnology **17**, 3873 (2006).
[52]J. Schmit, J. Reed, E. Novak, and J. Gimzewski, J. Opt. A: Pure Appl. Opt. **10**, 064001 (2008).
[53]M. Spletzer, A. Raman, H. Sumali, and J. Sullivan, Appl. Phys. Lett. **92**, 114102 (2008).
[54]J. Mertens, M. Álvarez, and J. Tamayo, Appl. Phys. Lett. **87**, 234102 (2005).
[55]M. Álvarez and J. Tamayo, Sens. Actuators B **106**, 687 (2005).
[56]G. Webber, G. Stevens, F. Grieser, R. Dagastine, and D. Chan, Nanotechnology **19**, 105709 (2008).
[57]M. Tortonese and M. Kirk, Micromachining and Imaging **3009**, 53 (1997).
[58]J. Mertens, M. Calleja, D. Ramos, A. Tarýn, and J. Tamayo, J. Appl. Phys. **101**, 034904 (2007).
[59]Y. Hu and W. Huang, J. Appl. Phys. **96**, 4154 (2004).
[60]J. Sader, J. Appl. Phys. **89**, 2911 (2001).
[61]V. Tabard-Cossa, M. Godin, I. Burgess, T. Monga, R. Lennox, and P. Grütter, Anal. Chem. **79**, 8136 (2007).
[62]M. Godin, V. Tabard-Cossa, Y. Miyahara, T. Monga, P. Williams, L. Beaulieu, R. Lennox, and P. Grutter, Nanotechnology **21**, 075501 (2010).
[63]M. Calleja, L. Carrascosa, A. Tarin, and J. Tamayo, Sens. Lett. **4**, 275 (2006).
[64]J. Floro, S. Hearne, J. Hunter, P. Kotula, E. Chason, S. Seel, and C. Thompson, J. Appl. Phys. **89**, 4886 (2001).
[65]M. Jose-Yacaman, C. Gutierrez-Wing, M. Miki, D. Yang, K. Piyakis, and E. Sacher, J. Phys. Chem. B **109**, 9703 (2005).
[66]G. Whitesides and P. Laibinis, Langmuir **6**, 87 (1990).
[67]R. Berger, E. Delamarche, H. Lang, C. Gerber, J. Gimzewski, E. Meyer, and H. Guntherodt, Science **276**, 2021 (1997).
[68]E. Cooper and G. Leggett, Langmuir **15**, 1024 (1999).

Downloaded 30 Jan 2012 to 161.111.180.103. Redistribution subject to AIP license or copyright; see http://rsi.aip.org/about/rights_and_permissions